Realization of pure gyration coupling in an on-chip superconducting microwave device

Zhiyin Tu [1,2] Violet Workman [3] Gaurav Bahl [4,5] and Alicia J. Kollár [2,6,7,*]

[1] Department of Electrical and Computer Engineering, University of Maryland, College Park, Maryland 20742, USA
[2] Joint Quantum Institute, University of Maryland, College Park, Maryland 20742, USA
[3] Department of Physics, University of Illinois at Urbana-Champaign, Urbana, Illinois 61801, USA
[4] Department of Mechanical Science and Engineering, University of Illinois at Urbana-Champaign, Urbana, Illinois 61801, USA
[5] Illinois Quantum Information Science and Technology Center, University of Illinois at Urbana-Champaign, Urbana, Illinois 61801, USA
[6] Department of Physics, University of Maryland, College Park, Maryland 20742, USA
[7] Quantum Materials Center, University of Maryland, College Park, Maryland 20742, USA

(Received 6 August 2025; accepted 17 December 2025; published 20 January 2026)

Synthetic materials that emulate tight-binding Hamiltonians have enabled a wide range of advances in topological and non-Hermitian physics. A crucial requirement in such systems is the engineering of nonreciprocal couplings and synthetic magnetic fields. More broadly, the development of these capabilities in a manner compatible with quantum-coherent degrees of freedom remains an outstanding challenge, particularly for superconducting circuits, which are highly sensitive to magnetic fields. Here, we demonstrate that *pure gyration*—a nonreciprocal coupling with exactly matched magnitude but nonreciprocal π phase contrast—can be realized between degenerate states using only spatiotemporal modulation. We first show the existence of continuous exceptional surfaces in modulation parameter space where coupling with arbitrarily large magnitude contrast can be achieved, with robust volumes of π phase contrast contained within. We then demonstrate that intersection of these volumes necessarily gives rise to continuous surfaces in parameter space where pure gyration is achieved. Our experiments are performed using microwave superconducting resonators that are modulated using dc superconducting quantum interference device arrays, and achieve isolation and pure gyration coupling with only superconducting circuit elements. However, our method is fully agnostic to physical implementation (classical or quantum) or frequency range and paves the way to realizing large-scale nonreciprocal metamaterials in any platform.

DOI: 10.1103/7mfg-5h1x

I. INTRODUCTION

Synthetic materials that emulate tight-binding Hamiltonians have proven instrumental in major advances in condensed matter and topological physics [1]. The generation of asymmetric couplings and effective magnetic fields in these synthetic materials has, in particular, enabled explorations of quantum Hall physics [2–11] and led to the discovery and first demonstrations of higher-order topological insulators [12–15], and the demonstrations of non-Hermitian skin effects [16–23] and topological funneling [24]. A specific requirement for nonreciprocal synthetic *quantum* materials—in which nonreciprocal couplings are combined with quantum-coherent degrees of freedom—is the ability to generate the asymmetry at low energy densities in an environment compatible with quantum control and coherent atoms or two-level systems. Superconducting circuits [25] are a prime candidate in this context, having realized lattice metamaterials [1,26,27] with reciprocal couplings.

While nonreciprocal couplers can be readily implemented in room-temperature electronics, mechanics, and microwave cavities [18,19,21,28,29], these approaches are incompatible for on-chip integration with superconducting quantum microwave circuits. To date, nonreciprocal coupling in superconducting circuits has focused almost entirely on the use of time modulation of *nondegenerate* states [30–33], which produces complex-valued couplings that impart equal and opposite phases in each direction and mimic the Hamiltonian of a charged particle in a magnetic field. However, spatiotemporal modulation of *degenerate* states provides a route to more general forms of nonreciprocal coupling [34–36]. Large *magnitude* contrast has been achieved using spatiotemporal modulation of degenerate states both in room-temperature [34], superconducting [35] microwave circuits and in photonics [36]. Recently, Ref. [36] showed that arbitrarily large magnitude contrast could be achieved, as well as couplings with opposite sign. However, because these results were in the weak modulation limit, one fundamental building block of nonreciprocal devices and non-Hermitian interactions has remained inaccessible: *pure gyration* coupling, in which a nonreciprocal π phase contrast is accompanied by perfect magnitude symmetry.

*Contact author: akollar@umd.edu

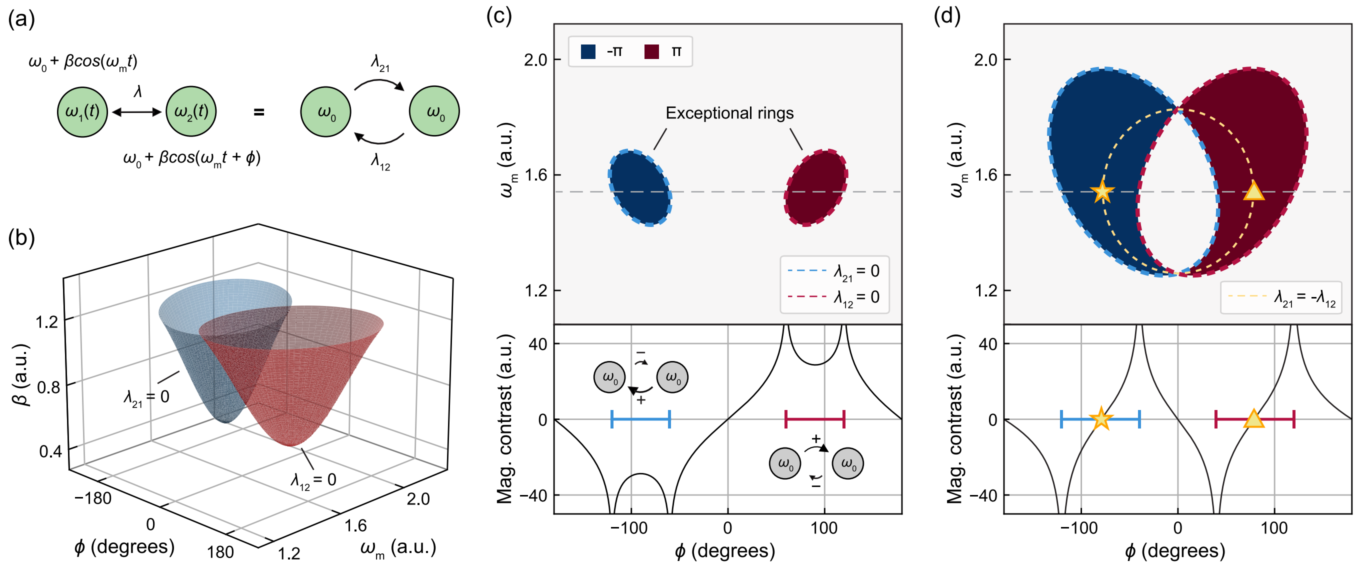

FIG. 1. Origin of pure gyration coupling through spatiotemporal modulation. (a) A pair of degenerate states with time modulated on-site energy can be shown to map to an equivalent static Hatano-Nelson (HN) model [36] that has $\lambda_{21} \neq \lambda_{12}$ when $\phi \neq 0^\circ, \pm 180^\circ$. An EP is obtained when either λ_{21} or λ_{12} goes to zero. (b) The 3D parameter space defined by β, ω_m, and ϕ reveals two exceptional surfaces corresponding to zeros of either coupling. (c) A plane cut of panel (b) taken at moderate β shows independent exceptional rings, inside which exactly one of the couplings becomes negative, indicating a relative π phase contrast. Log-scale plot of the coupling magnitude contrast along the gray dashed line shows zeros only at $\phi = 0^\circ, \pm 180^\circ$ and singularities at the EPs. (d) Above a critical modulation strength, the exceptional rings intersect, resulting in an alternation of the EPs along the cut indicated by the gray dashed line. This forces additional zeros in the magnitude contrast at nontrivial ϕ indicated by ☆ and △, where $\lambda_{21} = -\lambda_{12}$ (pure gyration) must occur. The gold dashed trajectory indicates the guaranteed existence of this pure gyration behavior over the entire ω_m range where the intersection occurs.

In this work, we demonstrate that pure gyration coupling between a pair of degenerate states can be produced through only spatiotemporal modulation. Our experimental system is comprised of a pair of degenerate superconducting microwave resonators, each of which contains a dedicated frequency modulator based on dc superconducting quantum interference devices (dc-SQUIDs) [37]. First, we go far beyond the exploration performed in photonics [36] and reveal a larger parameter space that supports exceptional point (EP) surfaces where giant coupling contrast can be achieved. At the EP, our device exhibits >58 dB microwave isolation, which is among the highest values reported in a chip-scale superconducting microwave device [32,35,38–42]. We then show that beyond these EPs lie islands of robustness where the phase nonreciprocity of the coupling holds perfectly at π and is extremely insensitive to parameter choice. And most excitingly, we find that once a critical modulation threshold is surpassed, these islands can intersect, and as a result, pure gyration coupling, with π phase nonreciprocity and exactly matched magnitude, can be found. The pure gyration effect is not an isolated singularity point and is also shown to be robust to parameter choice. The regimes of spatiotemporally modulated states revealed in this work are fully agnostic to implementation and should be accessible in any classical or quantum system.

Our experimental demonstration of pure gyration coupling is uniquely aided by the high dynamic range of the SQUID modulators and uses *only* superconducting circuit components compatible with superconducting-qubit quantum computing and no off-chip elements. When used in a one-dimensional chain with an even number of sites, the transmission response is that of a gyrator. As a result, our device also constitutes an integrated on-chip demonstration of pure gyration for quantum-microwave signals, which relies on frequency-modulated resonators alone, instead of using IQ mixers or hybrids, as was done in previous schemes for superconducting gyrators [43,44].

II. MODEL

We consider a simple case of two degenerate states with reciprocal mutual coupling λ [Fig. 1(a)]. The on-site energies are temporally modulated such that $\omega_1 = \omega_0 + \beta\cos(\omega_\mathrm{m} t)$ and $\omega_2 = \omega_0 + \beta\cos(\omega_\mathrm{m} t + \phi)$, where β is the modulation strength, ω_m is the modulation frequency, and ϕ is the differential modulation phase. In the analytically tractable case with only one upper and one lower sideband, it can be readily shown that, for fixed β and ω_m, $\phi = \pm 90^\circ$ maximizes the nonreciprocal transmission through the short chain [34]. More recently, it was shown that this system directly maps to an equivalent *static* case of two states with directional asymmetry in the linear response coupling coefficient at ω_0 producing $\lambda_{21} \neq \lambda_{12}$, even with an arbitrary number of sidebands, and thus implements the generalized Hatano-Nelson (HN) model [36]. The couplings can be described in the form $\lambda_{21,12} = \lambda(1 \pm \alpha)$, where real-valued $\alpha(\beta, \omega_\mathrm{m})$ is the degree of asymmetry that increases with larger β.

Qualitatively, the temporal modulation of the on-site energies generates a synthetic dimension in the frequency domain, which together with the physical axis of the chain forms a two-dimensional synthetic lattice [34,36] (see Secs. I and II in the Supplemental Material [45] for details). Due to the phase-staggering nature of the modulation, a synthetic mag-

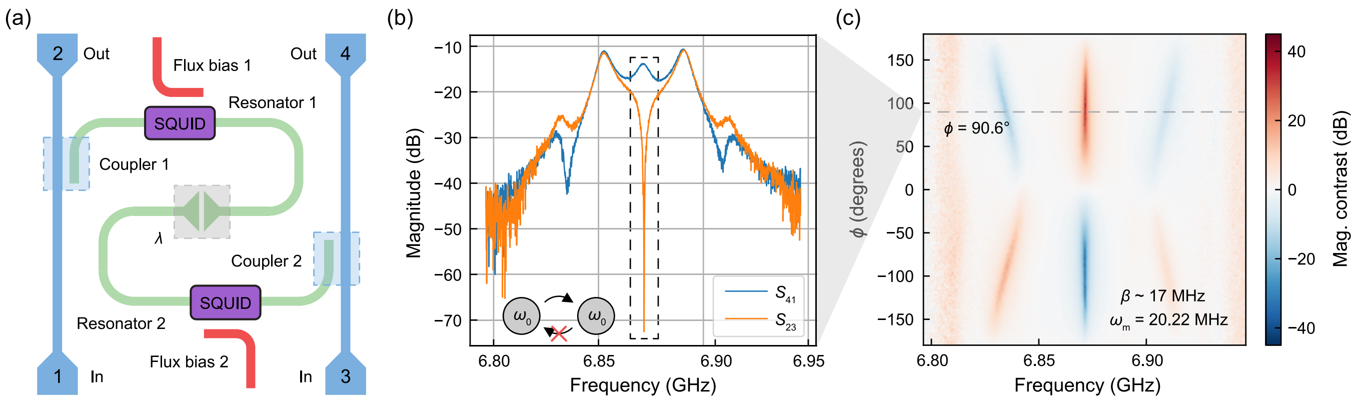

FIG. 2. Device schematic and measurement of giant magnitude contrast near an exceptional point. (a) Schematic of our experimental chip, composed of two degenerate superconducting resonators (nominal $\omega_0 = 6.8705$ GHz) with dc-SQUID frequency modulators that are controlled by independent flux bias lines. The capacitively coupled feedlines provide four input/output ports. Forward through-chain transmission is measured via S_{41} (backward transmission via S_{23}). Single-sided transmission measurements (S_{21} and S_{43}) are used for individual resonator characterization and device calibration (see Secs. IV and V in the Supplemental Material [45] for details). (b) Experimental measurements of forward and backward transmission demonstrating the system response near an EP, confirming $\lambda_{12} \to 0$ through observation of ≈58.6 dB giant magnitude contrast at ω_0. Here, we set $\beta \sim 17$ MHz, $\omega_m = 20.22$ MHz, and $\phi = 90.6°$, which is close to the bottom tip of the surfaces in Fig. 1(b). (c) A map of the magnitude contrast spectrum (defined as $|S_{41}| - |S_{23}|$) vs differential modulation phase ϕ, with color indicating the directionality. At ω_0, magnitude contrast exceeding 20 dB can be found over an 85° range of ϕ (similarly for negative ϕ with negative contrast).

netic field is generated within each plaquette of the synthetic lattice. It is interference between coupling paths involving many higher-order sidebands that gives rise to the equivalent non-Hermitian HN couplings [36]. For fixed $\phi = \pm 90°$, there exist arcs of EPs in the space mapped by β and ω_m, where $|\alpha| \to 1$ and one of the coupling coefficients $\lambda_{21,12}$ becomes exactly zero [36]. Beyond these arcs, we find $|\alpha| > 1$, which causes a sign inversion in the corresponding $\lambda_{21,12}$, producing in a system with gyration (nonreciprocity in phase) accompanied by finite magnitude contrast. From these previous studies, there seemed to be no possibility of the pure gyration case as no value of α can produce $\lambda_{21} = -\lambda_{12}$.

In this study, we permit ϕ to take any value and therefore generalize $\lambda_{21,12} = \lambda(1 - \alpha_{21,12})$ where $\alpha_{21,12}(\beta, \omega_m, \phi)$ are real valued (see Sec. II in the Supplemental Material [45] for details). This reveals continuous conelike exceptional surfaces within the three-dimensional space mapped by β, ω_m, and ϕ [Fig. 1(b)] that have not previously been considered. For moderate β, the EP first appears at $\phi = \pm 90°$, which corresponds to the tips of the two conelike disjoint exceptional surfaces and the cases discussed in Refs. [34,36]. As β increases, rings of EPs emerge in the ω_m–ϕ planes [Fig. 1(c)], corresponding to points where either of $\lambda_{21,12} \to 0$. Within these rings, the corresponding $\lambda_{21,12}$ becomes negative, implying a nonreciprocal coupling with exactly π phase contrast. Under these circumstances, the magnitude contrast (defined as $20 \log_{10} |\lambda_{21}/\lambda_{12}|$) *only* vanishes at trivial phases $\phi = 0°, \pm 180°$, whereas the π phase contrast only occurs between the EP singularities in other ranges of ϕ. As a result, π phase contrast is *always* accompanied by magnitude contrast.

Above a critical modulation strength, however, the exceptional surfaces enlarge and intersect [Figs. 1(b) and 1(d)], which is the key to achieving pure gyration coupling. Over the entire range of ω_m where the surfaces intersect, we now find an alternation of the EPs contributed by either ring [Fig. 1(d), bottom], which, due to the continuity of the magnitude contrast function, must force zeros in the contrast at nontrivial ϕ within the volume of influence of exactly one of the exceptional surfaces. Thus, *pure gyration* is guaranteed to appear over a continuous surface outside the intersecting volume. Since the pure gyration effect is required by continuity, it is not an isolated fine-tuned point, and the existence of pure gyration is robust to parameter choice (see Sec. II in the Supplemental Material [45] for a discussion of the strength of achievable pure gyration coupling). In the experiments that follow, we work with a two-site chain, and the transmission properties of the system at ω_0 are directly inherited from the effective couplings. We therefore refer to the couplings and the transmission characteristics interchangeably.

III. EXPERIMENTAL IMPLEMENTATION

We developed a superconducting microwave device consisting of two frequency-tunable resonators, as shown schematically in Fig. 2(a). The nominally identical coplanar waveguide transmission line resonators are capacitively coupled with static $\lambda \approx 16.4$ MHz. The tunability of the resonance frequency comes from a dc-SQUID array embedded in the middle of each resonator. Each SQUID serves as a flux-tunable inductance with

$$L_{\mathrm{SQUID}}(\Phi_e) = \frac{\hbar}{2eI_c\sqrt{1 + \gamma^2 + 2\gamma \cos\left(2\pi \frac{\Phi_e}{\Phi_0}\right)}}, \qquad (1)$$

where γ is the asymmetry factor between the two Josephson junctions that form the SQUID, I_c is the critical current for the smaller junction, Φ_e is the external magnetic flux threading the loop, and $\Phi_0 = h/2e$ is the superconducting magnetic flux quantum [46,47]. By putting N identical SQUIDs in series and forming an array, the total inductance L_{tot} becomes NL_{SQUID}

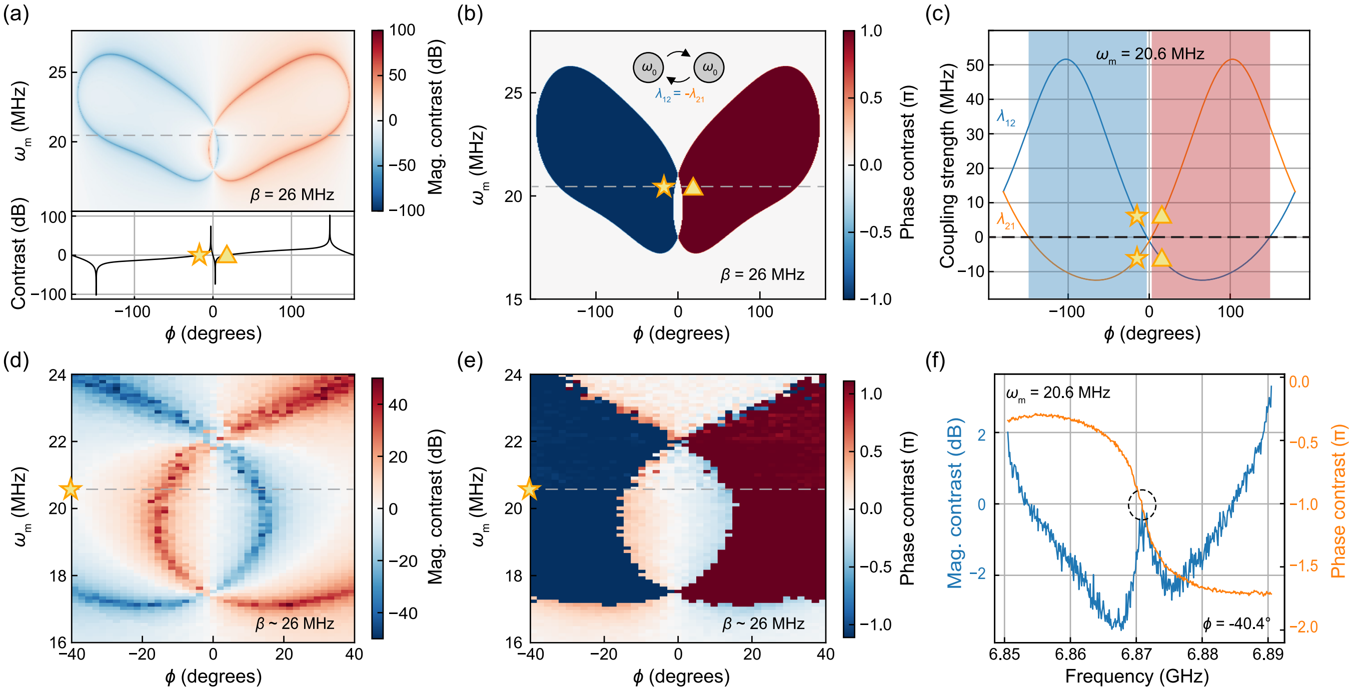

FIG. 3. Experimental realization of pure gyration coupling. (a) This numerical simulation of the magnitude contrast incorporates the experimentally measured properties of our test device to confirm that $\beta = 26\,\text{MHz}$ is above the critical modulation strength at which the exceptional rings (corresponding to either $\lambda_{21} = 0$ or $\lambda_{12} = 0$) intersect. ☆ and △ point out the new zeros in the magnitude contrast function for $\omega_m = 20.6\,\text{MHz}$. (b) The simulation predicts that these magnitude contrast zeros sit firmly within regions of π phase contrast. (c) We plot the calculated HN coupling coefficients $\lambda_{21,12}$ for the line cut at $\omega_m = 20.6\,\text{MHz}$, confirming that at either ☆ or △ we have $\lambda_{21} = -\lambda_{12}$. Blue and red shading indicates regions where λ_{21} and λ_{12} have opposite signs. (d), (e) Experimental measurements of magnitude contrast confirm the crossing of the exceptional rings, and the robust regions of π phase contrast within the rings. In panel (d), the regions in white indicate continuous lines on which there is no magnitude contrast. The white arcs that lie within the π phase contrast regions exhibit pure gyration. (f) A specific experimental measurement corresponding to ☆ ($\omega_m = 20.6\,\text{MHz}$ and $\phi = -40.4^\circ$) confirms the pure gyration effect where the magnitude contrast goes to zero while the phase contrast goes to π at ω_0 (highlighted in the black dashed circle).

(here, we choose $N = 2$). We supply both ac and dc bias voltages through the individual flux bias line next to the SQUID arrays such that the frequency of the resonators has a nominal value of $\omega_0 = 6.8705\,\text{GHz}$ with a superimposed sinusoidal modulation at ω_m. The device fabrication, measurement setup, and *in situ* calibrations are discussed in Secs. III and IV in the Supplemental Material [45].

The device features two capacitively coupled feedlines, one coupled to each resonator, giving rise to four input and output ports, as shown in Fig. 2(a). While not necessary for device operation, having two inputs and two outputs facilitates *in situ* characterization in the dilution refrigerator, where inputs and outputs must be routed though separate dedicated hardware (see Sec. IV in the Supplemental Material [45] for details). Transmission from port 1 to port 4 (S_{41}) and from port 3 to port 2 (S_{23}) pass through the resonator chain in the forward and backward directions, respectively. Differences between S_{41} and S_{23} (after *in situ* calibration) provide evidence for the nonreciprocity in the effective HN coupling coefficients [see Secs. IV and V in the Supplemental Material [45] for details).

We first confirm the existence of an EP near $\phi = \pm 90^\circ$ for moderate modulation strength, where strong nonreciprocal behavior is expected [34]. The measurements in Fig. 2(b), with modulation frequency $\omega_m = 20.22\,\text{MHz}$ and modulation strength $\beta \sim 17\,\text{MHz}$, confirm that an extremely large transmission magnitude contrast (>58 dB) can be obtained at ω_0 when one of the HN couplings approaches zero. In Fig. 2(c), we present additional measurements of the magnitude contrast over a large sweep of ϕ. These measurements confirm the robustness of the nonreciprocal behavior to the choice of modulation parameters. These data, taken along a line of fixed ω_m and β (with variable ϕ) that is tangent to the exceptional surfaces, show magnitude contrast at ω_0 in excess of 20 dB over an 85° range of ϕ (similarly for negative ϕ with negative contrast).

In Figs. 3(a)–3(c), we present numerical simulations of the device response at ω_0 for stronger β. Here, we find that $\beta = 26\,\text{MHz}$ is above the threshold modulation strength at which intersecting rings of EPs (corresponding to either $\lambda_{21} = 0$ or $\lambda_{12} = 0$) appear in the ω_m–ϕ plane. As predicted from the theoretical discussion in Fig. 1, we can identify points of interest for any choice of ω_m within the intersection range, 17.5–22 MHz, where magnitude contrast must go to zero while the phase contrast stays robustly at π. In Fig. 3(c), we select a slice at $\omega_m = 20.6\,\text{MHz}$ to identify these points of pure gyration HN coupling ($\lambda_{21} = -\lambda_{12}$) at nontrivial values of the differential modulation phase ϕ.

In Figs. 3(d) and 3(e), we present experimental measurements of the magnitude contrast and phase contrast at the intersection region. Continuity of the HN couplings and the magnitude contrast enforce the existence of a pure gyration point for *every* modulation frequency over the intersection since zeros of the magnitude contrast [white arcs in Fig. 3(d)] lie fully inside the π phase contrast regions [Fig. 3(e)] resulting from the rings of EPs. In Fig. 3(f), we present transmission measurements at a specific operating point indicated by ☆, where $\omega_m = 20.6$ MHz and $\phi = -40.4^\circ$. As expected, at ω_0 the measured phase contrast of π coincides with a near-zero magnitude contrast.

IV. CONCLUSION

The method presented here of achieving pure gyration and nonreciprocal couplings between degenerate degrees of freedom via spatiotemporal modulation is both simple and versatile, and can be extended to signal and information processing applications in *both* the classical and quantum regimes. The sign change of the coupling coefficients $\lambda_{21,12}$ when crossing the exceptional surfaces leads to a switchable π phase shift in transmission, which could be used to implement an extremely robust phase-shift keying protocol for classical telecommunications in which the phase shift is intrinsically protected, and control errors affect only the signal magnitude.

In the quantum regime, quantum computers based on superconducting qubits [25,48,49] rely on circulators and isolators to protect qubits from thermal radiation and amplifier backaction [48]. However, the current ferrite-based solutions are incompatible with on-chip integration due to their bulky form factor, which is orders of magnitude larger than the quantum processors they facilitate [49]. The device presented here, implemented using superconducting resonators in a dilution refrigerator, is compatible with superconducting qubits and adds desired capabilities to the toolbox of on-chip nonreciprocal devices for superconducting circuits [32,35,39–42,44]. In addition to being a fully on-chip realization of a gyrator for superconducting microwave devices, our device also realizes extremely high isolation (>58 dB), as well as the ability to dynamically reconfigure the direction of isolation. The combination of strong nonreciprocity and *in situ* reconfigurability makes this method ideal for narrower-band tasks such as shielding qubits from by-products of parametric amplifiers [48] or directional routing of quantum signals [41,50]. Furthermore, since superconducting transmon qubits [25] are formed using anharmonic oscillators, the simple spatiotemporal modulation method described here can also be employed between two degenerate qubits, rather than two resonators, where it should lead to nonreciprocal parametric two-qubit interactions.

ACKNOWLEDGMENTS

We thank Ashish Clerk, Oded Zilberberg, Andrew Daley, Penghao Zhu, Taylor Hughes, Jacopo Gliozzi, and Thomas Antonsen for helpful conversations and comments. This work was supported by Grants No. W911NF-23-1-0219 (ARO), No. W911NF-19-2-0181 (ARL), No. OMA-2120757 (NSF QLCI), and No. N00014-20-1-2325 (ONR MURI).

DATA AVAILABILITY

The data that support the findings of this article are not publicly available. The data are available from the authors upon reasonable request.

[1] I. Carusotto, A. A. Houck, A. J. Kollár, P. Roushan, D. I. Schuster, and J. Simon, Photonic materials in circuit quantum electrodynamics, Nat. Phys. **16**, 268 (2020).

[2] F. Guinea, M. I. Katsnelson, and A. Geim, Energy gaps and a zero-field quantum Hall effect in graphene by strain engineering, Nat. Phys. **6**, 30 (2010).

[3] J. Cho, D. G. Angelakis, and S. Bose, Fractional quantum Hall state in coupled cavities, Phys. Rev. Lett. **101**, 246809 (2008).

[4] Z. Wang, Y. D. Chong, J. D. Joannopoulos, and M. Soljačić, Reflection-free one-way edge modes in a gyromagnetic photonic crystal, Phys. Rev. Lett. **100**, 013905 (2008).

[5] J. Koch, A. A. Houck, K. L. Hur, and S. M. Girvin, Time-reversal-symmetry breaking in circuit-QED-based photon lattices, Phys. Rev. A **82**, 043811 (2010).

[6] Z. Wang, Y. Chong, J. D. Joannopoulos, and M. Soljačić, Observation of unidirectional backscattering-immune topological electromagnetic states, Nature (London) **461**, 772 (2009).

[7] M. C. Rechtsman, J. M. Zeuner, A. Tünnermann, S. Nolte, M. Segev, and A. Szameit, Strain-induced pseudomagnetic field and photonic Landau levels in dielectric structures, Nat. Photonics **7**, 153 (2013).

[8] M. Aidelsburger, M. Atala, S. Nascimbène, S. Trotzky, Y.-A. Chen, and I. Bloch, Experimental realization of strong effective magnetic fields in an optical lattice, Phys. Rev. Lett. **107**, 255301 (2011).

[9] M. Aidelsburger, M. Atala, M. Lohse, J. T. Barreiro, B. Paredes, and I. Bloch, Realization of the Hofstadter Hamiltonian with ultracold atoms in optical lattices, Phys. Rev. Lett. **111**, 185301 (2013).

[10] T. Ozawa, H. M. Price, N. Goldman, O. Zilberberg, and I. Carusotto, Synthetic dimensions in integrated photonics: From optical isolation to four-dimensional quantum Hall physics, Phys. Rev. A **93**, 043827 (2016).

[11] M. Lohse, C. Schweizer, H. M. Price, O. Zilberberg, and I. Bloch, Exploring 4D quantum Hall physics with a 2D topological charge pump, Nature (London) **553**, 55 (2018).

[12] W. A. Benalcazar, B. A. Bernevig, and T. L. Hughes, Quantized electric multipole insulators, Science **357**, 61 (2017).

[13] C. W. Peterson, W. A. Benalcazar, T. L. Hughes, and G. Bahl, A quantized microwave quadrupole insulator with topologically protected corner states, Nature (London) **555**, 346 (2018).

[14] M. Serra-Garcia, V. Peri, R. Süsstrunk, O. R. Bilal, T. Larsen, L. G. Villanueva, and S. D. Huber, Observation of a phononic quadrupole topological insulator, Nature (London) **555**, 342 (2018).

[15] S. S. Yamada, T. Li, M. Lin, C. W. Peterson, T. L. Hughes, and G. Bahl, Bound states at partial dislocation defects in multipole higher-order topological insulators, Nat. Commun **13**, 2035 (2022).

[16] N. Hatano and D. R. Nelson, Localization transitions in non-Hermitian quantum mechanics, Phys. Rev. Lett. **77**, 570 (1996).
[17] N. Hatano and D. R. Nelson, Non-Hermitian delocalization and eigenfunctions, Phys. Rev. B **58**, 8384 (1998).
[18] M. Brandenbourger, X. Locsin, E. Lerner, and C. Coulais, Non-reciprocal robotic metamaterials, Nat. Commun **10**, 4608 (2019).
[19] T. Helbig, T. Hofmann, S. Imhof, M. Abdelghany, T. Kiessling, L. Molenkamp, C. Lee, A. Szameit, M. Greiter, and R. Thomale, Generalized bulk–boundary correspondence in non-Hermitian topolectrical circuits, Nat. Phys. **16**, 747 (2020).
[20] N. Okuma, K. Kawabata, K. Shiozaki, and M. Sato, Topological origin of non-Hermitian skin effects, Phys. Rev. Lett. **124**, 086801 (2020).
[21] L. Zhang, Y. Yang, Y. Ge, Y.-J. Guan, Q. Chen, Q. Yan, F. Chen, R. Xi, Y. Li, D. Jia, *et al.*, Acoustic non-Hermitian skin effect from twisted winding topology, Nat. Commun. **12**, 6297 (2021).
[22] Y. G. Liu, Y. Wei, O. Hemmatyar, G. G. Pyrialakos, P. S. Jung, D. N. Christodoulides, and M. Khajavikhan, Complex skin modes in non-Hermitian coupled laser arrays, Light Sci. Appl. **11**, 336 (2022).
[23] Z. Gao, X. Qiao, M. Pan, S. Wu, J. Yim, K. Chen, B. Midya, L. Ge, and L. Feng, Two-dimensional reconfigurable non-Hermitian gauged laser array, Phys. Rev. Lett. **130**, 263801 (2023).
[24] S. Weidemann, M. Kremer, T. Helbig, T. Hofmann, A. Stegmaier, M. Greiter, R. Thomale, and A. Szameit, Topological funneling of light, Science **368**, 311 (2020).
[25] A. Blais, A. L. Grimsmo, S. M. Girvin, and A. Wallraff, Circuit quantum electrodynamics, Rev. Mod. Phys. **93**, 025005 (2021).
[26] A. A. Houck, H. E. Türeci, and J. Koch, On-chip quantum simulation with superconducting circuits, Nat. Phys. **8**, 292 (2012).
[27] R. Ma, B. Saxberg, C. Owens, N. Leung, Y. Lu, J. Simon, and D. I. Schuster, A dissipatively stabilized Mott insulator of photons, Nature (London) **566**, 51 (2019).
[28] J. S. Salcedo-Gallo, M. Burgelman, V. P. Flynn, A. S. Carney, M. Hamdan, T. Gerg, D. C. Smallwood, L. Viola, and M. Fitzpatrick, Demonstration of a tunable non-Hermitian nonlinear microwave dimer, Nat. Commun. **16**, 7193 (2025).
[29] C. Owens, A. LaChapelle, B. Saxberg, B. M. Anderson, R. Ma, J. Simon, and D. I. Schuster, Quarter-flux Hofstadter lattice in a qubit-compatible microwave cavity array, Phys. Rev. A **97**, 013818 (2018).
[30] P. Roushan, C. Neill, A. Megrant, Y. Chen, R. Babbush, R. Barends, B. Campbell, Z. Chen, B. Chiaro, A. Dunsworth, *et al.*, Chiral ground-state currents of interacting photons in a synthetic magnetic field, Nat. Phys. **13**, 146 (2017).
[31] I. T. Rosen, S. Muschinske, C. N. Barrett, A. Chatterjee, M. Hays, M. A. DeMarco, A. H. Karamlou, D. A. Rower, R. Das, D. K. Kim, *et al.*, A synthetic magnetic vector potential in a 2D superconducting qubit array, Nat. Phys. **20**, 1881 (2024).
[32] F. Lecocq, L. Ranzani, G. A. Peterson, K. Cicak, R. W. Simmonds, J. D. Teufel, and J. Aumentado, Nonreciprocal microwave signal processing with a field-programmable Josephson amplifier, Phys. Rev. Appl. **7**, 024028 (2017).
[33] I. T. Rosen, S. Muschinske, C. N. Barrett, D. A. Rower, R. Das, D. K. Kim, B. M. Niedzielski, M. Schuldt, K. Serniak, M. E. Schwartz, J. L. Yoder, J. A. Grover, and W. D. Oliver, Flat-band (De)localization emulated with a superconducting qubit array, Phys. Rev. X **15**, 021091 (2025).
[34] C. W. Peterson, W. A. Benalcazar, M. Lin, T. L. Hughes, and G. Bahl, Strong nonreciprocity in modulated resonator chains through synthetic electric and magnetic fields, Phys. Rev. Lett. **123**, 063901 (2019).
[35] Y. Zhuang, C. Gaikwad, D. Kowsari, K. Murch, and A. Nagulu, Superconducting isolators based on time-modulated coupled-resonator systems, Phys. Rev. Appl. **21**, 054061 (2024).
[36] O. E. Örsel, J. Noh, P. Zhu, J. Yim, T. L. Hughes, R. Thomale, and G. Bahl, Giant nonreciprocity and gyration through modulation-induced Hatano-Nelson coupling in integrated photonics, Phys. Rev. Lett. **134**, 153801 (2025).
[37] M. Tinkham, *Introduction to Superconductivity* (Dover Publications, Garden City, New York, 2004).
[38] B. Abdo, O. Jinka, N. T. Bronn, S. Olivadese, and M. Brink, High-fidelity qubit readout using interferometric directional Josephson devices, PRX Quantum **2**, 040360 (2021).
[39] M. Beck, M. Selvanayagam, A. Carniol, S. Cairns, and C. Mancini, Wideband Josephson parametric isolator, Phys. Rev. Appl. **20**, 034054 (2023).
[40] B. J. Chapman, E. I. Rosenthal, J. Kerckhoff, B. A. Moores, L. R. Vale, J. Mates, G. C. Hilton, K. Lalumiere, A. Blais, and K. Lehnert, Widely tunable on-chip microwave circulator for superconducting quantum circuits, Phys. Rev. X **7**, 041043 (2017).
[41] X. Cao, A. Irfan, M. Mollenhauer, K. Singirikonda, and W. Pfaff, Parametrically controlled chiral interface for superconducting quantum devices, Phys. Rev. Appl. **22**, 064023 (2024).
[42] N. R. Bernier, L. D. Toth, A. Koottandavida, M. A. Ioannou, D. Malz, A. Nunnenkamp, A. Feofanov, and T. Kippenberg, Nonreciprocal reconfigurable microwave optomechanical circuit, Nat. Commun. **8**, 604 (2017).
[43] E. I. Rosenthal, B. J. Chapman, A. P. Higginbotham, J. Kerckhoff, and K. W. Lehnert, Breaking Lorentz reciprocity with frequency conversion and delay, Phys. Rev. Lett. **119**, 147703 (2017).
[44] B. Abdo, M. Brink, and J. M. Chow, Gyrator operation using Josephson mixers, Phys. Rev. Appl. **8**, 034009 (2017).
[45] See Supplemental Material at http://link.aps.org/supplemental/10.1103/7mfg-5h1x for additional information on detailed theoretical derivations, effective Hatano-Nelson mapping, device fabrication methods, experimental setup, and *in situ* parameter calibrations, which includes Refs. [51,52].
[46] M. Pechal, J.-C. Besse, M. Mondal, M. Oppliger, S. Gasparinetti, and A. Wallraff, Superconducting switch for fast on-chip routing of quantum microwave fields, Phys. Rev. Appl. **6**, 024009 (2016).
[47] P. Krantz, M. Kjaergaard, F. Yan, T. P. Orlando, S. Gustavsson, and W. D. Oliver, A quantum engineer's guide to superconducting qubits, Appl. Phys. Rev. **6**, 021318 (2019).

[48] J. Aumentado, Superconducting parametric amplifiers: The state of the art in Josephson parametric amplifiers, IEEE Microwave Mag. **21**, 45 (2020).

[49] S. Krinner, S. Storz, P. Kurpiers, P. Magnard, J. Heinsoo, R. Keller, J. Luetolf, C. Eichler, and A. Wallraff, Engineering cryogenic setups for 100-qubit scale superconducting circuit systems, EPJ Quantum Technol. **6**, 2 (2019).

[50] B. Kannan, A. Almanakly, Y. Sung, A. Di Paolo, D. A. Rower, J. Braumüller, A. Melville, B. M. Niedzielski, A. Karamlou, K. Serniak, *et al.*, On-demand directional microwave photon emission using waveguide quantum electrodynamics, Nat. Phys. **19**, 394 (2023).

[51] W. Suh, Z. Wang, and S. Fan, Temporal coupled-mode theory and the presence of non-orthogonal modes in lossless multimode cavities, IEEE J. Quantum Electron. **40**, 1511 (2004).

[52] C. Manolatou, M. Khan, S. Fan, P. R. Villeneuve, H. Haus, and J. Joannopoulos, Coupling of modes analysis of resonant channel add-drop filters, IEEE J. Quantum Electron. **35**, 1322 (1999).